Acta Crystallographica Section D
Biological Crystallography
ISSN 0907-4449

Direct inter-subdomain interactions switch between the closed and open forms of the Hsp70 nucleotide-binding domain in the nucleotide-free state

Meiri Shida,[a,b]‡ Akihiko Arakawa,[a,b] Ryohei Ishii,[a,b]§ Seiichiro Kishishita,[b]¶ Tetsuo Takagi,[b] Mutsuko Kukimoto-Niino,[b] Sumio Sugano,[c] Akiko Tanaka,[b] Mikako Shirouzu[b] and Shigeyuki Yokoyama[a,b]*

[a]Department of Biophysics and Biochemistry, Graduate School of Science, The University of Tokyo, 7-3-1 Hongo, Bunkyo-ku, Tokyo 113-0033, Japan, [b]RIKEN Systems and Structural Biology Center, 1-7-22 Suehiro-cho, Tsurumi, Yokohama 230-0045, Japan, and [c]Laboratory of Functional Genomics, Department of Medical Genome Sciences, Graduate School of Frontier Sciences, The University of Tokyo, 4-6-1 Shirokanedai, Minato-ku, Tokyo 108-8639, Japan

‡ Present address: Chugai Pharmaceutical Co. Ltd, 1-135 Komakado, Gotemba, Shizuoka 412-8513, Japan.
§ Present address: Department of Pathology and Laboratory Medicine, Weill Medical College of Cornell University, 1300 York Avenue C-458C, New York, NY 10021, USA.
¶ Present address: Novozymes Japan Ltd, 1-3 Nakase, Mihama-ku, Chiba 261-8501, Japan.

Correspondence e-mail: yokoyama@biochem.s.u-tokyo.ac.jp

Received 4 September 2009
Accepted 15 December 2009

PDB References: Hsp70 nucleotide-binding domain, nucleotide-free state, 2e88; AMPPNP-bound state, 2e8a.

The 70 kDa heat-shock proteins (Hsp70s) are highly conserved chaperones that are involved in several cellular processes, such as protein folding, disaggregation and translocation. In this study, the crystal structures of the human Hsp70 nucleotide-binding domain (NBD) fragment were determined in the nucleotide-free state and in complex with adenosine 5′-(β,γ-imido)triphosphate (AMPPNP). The structure of the nucleotide-free NBD fragment is similar to that of the AMPPNP-bound NBD fragment and is designated as the 'closed form'. In the nucleotide-free NBD fragment the closed form is intrinsically supported through interactions between Tyr15, Lys56 and Glu268 which connect subdomains IA, IB and IIB at the centre of the protein. Interaction with the substrate-binding domain (SBD) of Hsp70 or the BAG domain of BAG1 impairs this subdomain connection and triggers the rotation of subdomain IIA around a hydrophobic helix from subdomain IA. The subdomain rotation is limited by Asp199 and Asp206 from subdomain IIA and clearly defines the open form of the NBD. The open form is further stabilized by a new interaction between Gly230 from subdomain IIB and Ser340 from subdomain IIA. The structure of the NBD in the nucleotide-free state is determined by switching of the inter-subdomain interactions.

1. Introduction

In response to a wide variety of stresses, including elevated temperatures, all living organisms synthesize a specific subset of proteins called heat-shock proteins (HSPs; DiDomenico *et al.*, 1982). The HSPs are divided into families according to their molecular masses; the 70 kDa heat-shock proteins (Hsp70s) constitute one of the major HSP families in prokaryotic and eukaryotic organisms (Hunt & Morimoto, 1985; Lindquist & Craig, 1988). *Escherichia coli* has three Hsp70 homologues, DnaK, HscA (Hsc66) and HscC (Hsc62), whereas there are more than ten human Hsp70 genes, including the heat-shock-inducible Hsp70 (or Hsp72) and the housekeeping 70 kDa heat-shock cognate protein (Hsc70; Goldfarb *et al.*, 2006). Human Hsp70s are involved in programmed cell death, differentiation, proliferation, signal transduction, cell-cycle regulation and senescence (Kao *et al.*, 1985; Zakeri & Wolgemuth, 1987; Niedzwiecki *et al.*, 1991; Jaattela, 1993; Multhoff *et al.*, 1999; Nylandsted *et al.*, 2000) and have been implicated in many kinds of pathological processes, such as oncogenesis, neurodegeneration and autoimmune disease (Hantschel *et al.*, 2000; Imai *et al.*, 2002; Millar *et al.*, 2003; Kalia *et al.*, 2004).

Hsp70s consist of a 44 kDa nucleotide-binding domain (NBD), an 18 kDa substrate-binding domain (SBD) and a 10 kDa C-terminal domain (CTD). The central substrate-

binding domain exhibits protein substrate-binding and regulatory activities (Wilbanks *et al.*, 1995). The tertiary structures of SBD fragments of *E. coli* DnaK and HscA and rat Hsc70 have been analyzed, particularly with respect to their interactions with substrate peptides (Wang *et al.*, 1998; Morshauser *et al.*, 1999; Pellecchia *et al.*, 2000; Cupp-Vickery *et al.*, 2004). In the SBD, the β-sandwich subdomain (SBDβ) binds the substrate, whereas the α-helical subdomain (SBDα) serves as a lid for the substrate-bound SBDβ. Moreover, the SBDα reportedly interacts with the NBD for functional regulation (Zhu *et al.*, 1996; Mayer *et al.*, 2000; Swain *et al.*, 2007). The C-terminal domain (CTD) is α-helical and plays a role in self-association in both *E. coli* DnaK and rat Hsc70 (Wilbanks *et al.*, 1995; Ungewickell *et al.*, 1997; Chou *et al.*, 2003).

The nucleotide-binding domain binds and hydrolyzes ATP (Ha & McKay, 1994). The NBD fragments from bovine Hsc70, human Hsp70 and rat Hsp70 in complex with ADP or the nonhydrolyzable ATP analogue AMPPNP have similar structures (Flaherty *et al.*, 1990, 1994; O'Brien *et al.*, 1996; Zhu *et al.*, 1996; Harrison *et al.*, 1997; Sriram *et al.*, 1997; Osipiuk *et al.*, 1999; Sondermann *et al.*, 2001; Jiang *et al.*, 2005, 2007; Liu & Hendrickson, 2007). The NBD consists of four subdomains, IA, IB, IIA and IIB, and the adenine moiety and the phosphate groups of the bound nucleotides interact with subdomains IIA and IIB and with subdomains IA and IIA, respectively. This conformation of the NBD is designated in the following as the 'closed form'. In the structure of a fragment of *Geobacillus kaustophilus* DnaK lacking the CTD (or the NBD-SBD fragment), the ADP-bound NBD exists in the closed form and is totally separated from the SBD (Chang *et al.*, 2008). Furthermore, the ADP-bound NBD in the solution NMR structure of the full-length *E. coli* DnaK also adopts the closed form (Bertelsen *et al.*, 2009).

On the other hand, in a complex with the Bcl2-associated athanogene (BAG) domain of human BAG-1, the nucleotide-free state of the bovine Hsc70 NBD in exists in another form in which the nucleotide-binding pocket is more open than in the closed form (the 'open form'; Sondermann *et al.*, 2001; Xu *et al.*, 2008). This open-form conformation explains how BAG-1 serves as a nucleotide-exchange factor for Hsp70s. The open form is also adopted by the NBD portion of the NBD-SBD fragment of bovine Hsc70 in the nucleotide-free state.

Yeast Sse1 is a member of the Hsp110 family (one of the subfamilies of the Hsp70 family) and serves as a nucleotide-exchange factor for Hsp70s rather than a chaperone (Easton *et al.*, 2000; Raviol *et al.*, 2006). In the structure of ATP-bound Sse1 in a construct containing both the NBD and SBD, the NBD portion assumes the 'closed form', as in the nucleotide-bound NBD isolated from the Hsp70/Hsc70 chaperones (Liu & Hendrickson, 2007). In the crystal structures of human Hsp70 NBD and bovine Hsc70 NBD-SBD in complex with Sse1–ATP, the NBD of Hsp70/Hsc70 adopts a conformation (designated in the following as the 'open* form') that is more expanded than the above-mentioned open form (Polier *et al.*, 2008). The Sse1-bound NBD-SBD of Hsc70 is still bound by ADP and interacts with the adenine moiety but not with the phosphate groups, which is consistent with the open state (Schuermann *et al.*, 2008).

In the present study, we determined the crystal structure of the nucleotide-free NBD fragment of human Hsp70 at 1.80 Å resolution. The AMPPNP-bound structure was also solved at 1.77 Å resolution. Intriguingly, the nucleotide-free NBD fragment adopts a closed form quite similar to the nucleotide-bound form. We identified the direct subdomain–subdomain interactions at the centre of the NBD as characteristic of the closed form: hydrogen-bonding and electrostatic interactions of Glu268 from subdomain IIB with Tyr15 from subdomain IA and with Lys56 from subdomain IB, respectively. Therefore, we propose that the NBD in the nucleotide-free state intrinsically exists in an equilibrium between the closed and open forms. In contrast, the reported nucleotide-free Hsp70-family proteins in the open form lack the central subdomain interactions Tyr15–Glu268–Lys56 but characteristically exhibit an alternative hydrogen-bonding interaction between Gly230 from subdomain IIB and Ser340 from subdomain IIA. Consequently, in the nucleotide-free state of the NBD the switch between the closed and open forms is associated with changes in the central inter-subdomain interactions.

2. Materials and methods

2.1. Subcloning of the human Hsp70 ATPase-domain fragment into the expression vector

The NBD fragment (residues 1–388) was constructed by PCR amplification of the full-length gene and was cloned into pENTR/TEV/D-TOPO (Invitrogen). After verification of the sequence by DNA sequencing, the expression vector was constructed using Gateway technology (Invitrogen) with the pET-32/Gateway vector, which was inserted into Gateway reading frame cassette A (Invitrogen) in pET-32a(+) (Novagen).

2.2. Protein expression and purification

The wild-type (WT) NBD and mutant NBD expression plasmids were introduced into *E. coli* strain Rosetta (DE3). The cells were grown in Luria–Bertani broth at 310 K and protein expression was induced at an optical density of 0.6 at 600 nm by the addition of isopropyl β-D-1-thiogalactopyranoside to a final concentration of 0.3 m*M*. The cells were harvested by centrifugation and suspended in 20 m*M* sodium phosphate buffer pH 8.0 containing 500 m*M* NaCl, 5 m*M* imidazole and 5 m*M* β-mercaptoethanol.

The cells were lysed by sonication and clarified by centrifugation. The clarified lysate was applied onto a His-Trap column (GE Healthcare) equilibrated in the same buffer and the protein was eluted with an increasing imidazole gradient in the same buffer. Fractions containing substantial amounts of the target protein were pooled and TEV (tobacco etch virus) protease was added to the protein solution. The sample was dialyzed at 277 K against 20 m*M* sodium phosphate buffer pH 8.0 containing 50 m*M* NaCl, 30 m*M* imidazole and 5 m*M* β-mercaptoethanol and was loaded onto a HisTrap column to remove the TEV protease and the cleaved His tag. The sample

was dialyzed at 277 K against 20 m*M* sodium phosphate buffer pH 8.0 containing 5 m*M* β-mercaptoethanol, applied onto a HiTrap Blue column (GE Healthcare) equilibrated in the same buffer and eluted with a gradient of increasing NaCl concentration in the same buffer. The fractions containing the 43 kDa NBD protein were pooled and dialyzed at 277 K against 20 m*M* Tris–HCl buffer pH 8.0 containing 25 m*M* NaCl and 5 m*M* β-mercaptoethanol and were loaded onto a MonoQ ion-exchange column (GE Healthcare). The bound protein was eluted using an NaCl gradient in the same buffer. Further purification was achieved using a Superdex 200 gel-filtration column (GE Healthcare) equilibrated with 20 m*M* Tris–HCl buffer pH 8.0 containing 150 m*M* NaCl and 5 m*M* β-mercaptoethanol. The fractions containing the NBD protein were pooled and concentrated to 10 mg ml^{-1} by centrifugation in an Amicon Ultra filter (Millipore).

2.3. HPLC analysis

20 μ*M* ATP and ADP (Sigma) in 20 m*M* Tris–HCl buffer pH 8.0 containing 150 m*M* NaCl and 5 m*M* β-mercaptoethanol were used as standard substances. The NBD-fragment samples purified with and without the HiTrap Blue column were both denatured by 0.6 *M* ice-cold perchloric acid and centrifuged at 15 000 rev min^{-1} for 15 min to remove the protein. The supernatants were neutralized using 4 *M* KOH and were centrifuged to remove the potassium perchlorate. Aliquots (10 µl) of the cleared supernatants were applied onto a Supelcosil LC-18-T (5 µm) RP column (4.6 × 250 mm, Supelco). 100 m*M* KH_2PO_4 buffer pH 6.0 containing 4%(*v*/*v*) methanol was used as the running buffer at a flow rate of 1 ml min^{-1}. The absorbencies of ATP and ADP were monitored at 256 nm.

2.4. Crystallization

Crystallization of the nucleotide-free NBD protein was performed at 293 K using the 96-well sitting-drop vapour-diffusion method. Aliquots (100 µl) of the reservoir solutions were dispensed into 96-well Intelli-Plates (Art Robbins Instruments) using a Biomek FX Workstation (Beckman Coulter) and 0.5 µl portions of the reservoir solutions were mixed with 0.5 µl protein solution (10 mg ml^{-1}). The crystallization drops were incubated and observed at 293 K using the Crystal Farm 400 imaging system (NEXUS Biosystems Inc.). To obtain crystals of the AMPPNP-bound NBD protein, $MgCl_2$ and AMPPNP, both at 5 m*M*, were added to the protein solution prior to crystallization and protein crystallization was performed in the same manner. In about one week, crystals of both nucleotide-free and AMPPNP-bound NBD protein were obtained using the reservoir solution 0.1 *M* HEPES buffer pH 7.5 containing 25% PEG 3350.

2.5. Data collection, model building and refinement

All diffraction data were recorded at 93 K using the reservoir solution containing 15% PEG 400 as a cryoprotectant. Diffraction data for the unliganded crystal were recorded using a CCD detector on the BL5-A beamline at the Photon Factory (Tsukuba, Japan). Diffraction data for the AMPPNP-bound crystal were recorded using a CCD detector on the BL26B2 beamline at SPring-8 (Harima, Japan). Data sets were processed with the *HKL* software package and were scaled with *SCALEPACK* (Otwinowski & Minor, 1997).

The crystal structures were solved by the molecular-replacement method using the program *MOLREP* (Vagin & Teplyakov, 1997). The initial model was the human Hsp70 NBD in the ADP-bound state (PDB code 1hjo; Osipiuk *et al.*, 1999). After several rounds of manual revision of the model using *WinCoot* (Emsley & Cowtan, 2004) and refinement using *CNS* (Brünger *et al.*, 1998) the R and $R_{\rm free}$ values converged, as shown in Table 1. The qualities of the refined models were inspected using *PROCHECK* (Laskowski *et al.*, 1993).

Table 1
Crystallographic data and refinement statistics.

Values in parentheses are for the highest resolution shell.

Structure	Nucleotide-free state	Complex with AMPPNP
Data collection		
Beamline	Photon Factory BL-5A	SPring-8 BL26B2
Space group	$P2_12_12_1$	$P2_12_12_1$
Unit-cell parameters (Å)	a = 46.01, b = 62.11, c = 143.07	a = 45.49, b = 62.22, c = 143.04
Resolution (Å)	50–1.80 (1.91–1.80)	50–1.77 (1.88–1.77)
No. of reflections	369583	282942
No. of unique reflections	38793	40539
Redundancy	9.5	7.0
Completeness (%)	100 (100)	99.9 (99.8)
$I/\sigma(I)$	22.6 (2.7)	12.3 (1.2)
$R_{\rm merge}$† (%)	0.1 (7.8)	0.1 (7.4)
Refinement statistics		
Resolution (Å)	31.00–1.80	46.94–1.77
No. of reflections	38685	40453
No. of protein atoms	2955	2947
No. of water molecules	416	416
No. of zinc ions	1	0
No. of magnesium ions	0	1
No. of AMPPNP molecules	0	1
$R_{\rm work}/R_{\rm free}$‡ (%)	19.3/23.9	18.5/23.0
R.m.s.d. bonds (Å)	0.009	0.009
R.m.s.d. angles (°)	1.50	1.40
Average isotropic B value (Å^2)	25.50	23.00
Ramachandran plot		
Most favoured regions (%)	91.7	93.2
Additional allowed regions (%)	8.3	6.8
PDB code	2e88	2e8a

† $R_{\rm merge} = \sum_{hkl}\sum_i |I_i(hkl) - \langle I(hkl)\rangle|/\sum_{hkl}\sum_i I_i(hkl)$, where $I(hkl)$ is the observed intensity of reflections. ‡ $R_{\rm work}$, $R_{\rm free} = \sum_{hkl} ||F_{\rm obs}| - |F_{\rm calc}||/\sum_{hkl} |F_{\rm obs}|$, where the crystallographic R factor is calculated including and excluding refinement reflections. In each refinement, free reflections consist of 5% of the total number of reflections

3. Results and discussion

3.1. Purification of the nucleotide-free NBD fragment of human Hsp70

To obtain the recombinant NBD fragment in the nucleotide-free state we utilized a HiTrap Blue column, in which the ligand (Cibacron Blue F3G-A) probably binds to the

nucleotide-binding pocket, and eluted the NBD fragment from the column using a salt-concentration gradient. The NBD fragment purified by chromatography on columns including the HiTrap Blue column contained no detectable amounts of ATP and ADP. In contrast, ADP was detected in the NBD fragment purified without using the HiTrap Blue column (Fig. 1*a*).

3.2. Structure determination

The structure of the NBD fragment in the nucleotide-free state was solved by the molecular-replacement method, using the human Hsp70 NBD in the ADP-bound state (PDB code 1hjo; ADP-bound NBD; Osipiuk *et al.*, 1999) as the search model, and was refined against data to 1.80 Å resolution (Fig. 1*b*). In addition, we solved the structure of the NBD in the AMPPNP-bound state by the same method, using the structure of the nucleotide-free NBD as the starting model, and refined it against data to 1.77 Å resolution (Fig. 1*c*). The data statistics are shown in Table 1. The coordinates are of high quality; over 90% of the residues are in the most favoured regions and the other residues are in the additional allowed regions of the Ramachandran plot for both structures.

In the structure of the AMPPNP-bound NBD, an AMPPNP molecule and an Mg^{2+} ion are bound in the nucleotide-binding pocket (Fig. 1*c*). Subdomains IA (residues 3–39, 116–188 and 361–384), IB (residues 40–115), IIA (residues 189–228 and 307–360) and IIB (residues 229–306) (Flaherty *et al.*, 1990) are labelled in both structures.

3.3. Overall structures

It is remarkable that the overall structure of the nucleotide-free NBD of human Hsp70 is highly superimposable on that of

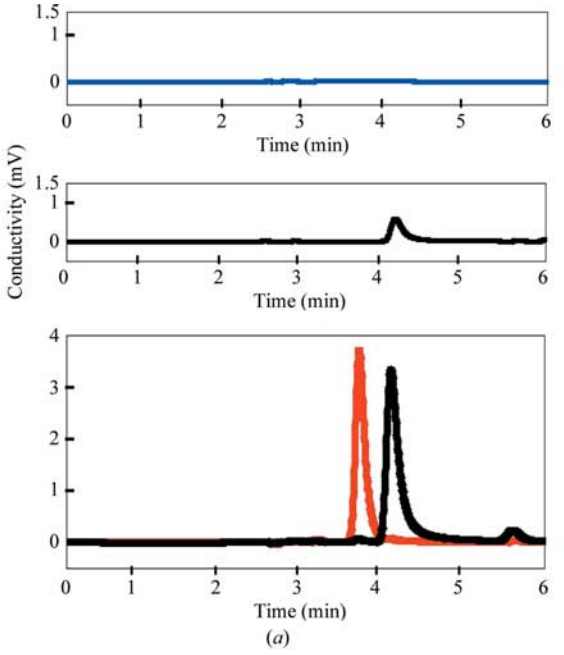

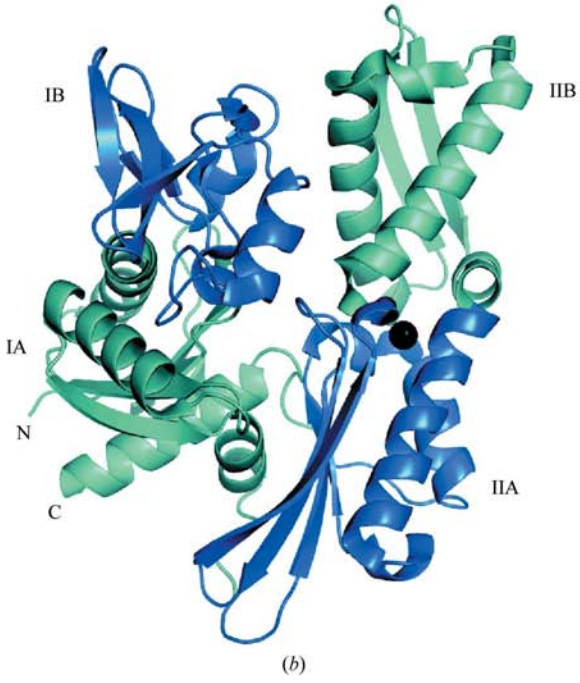

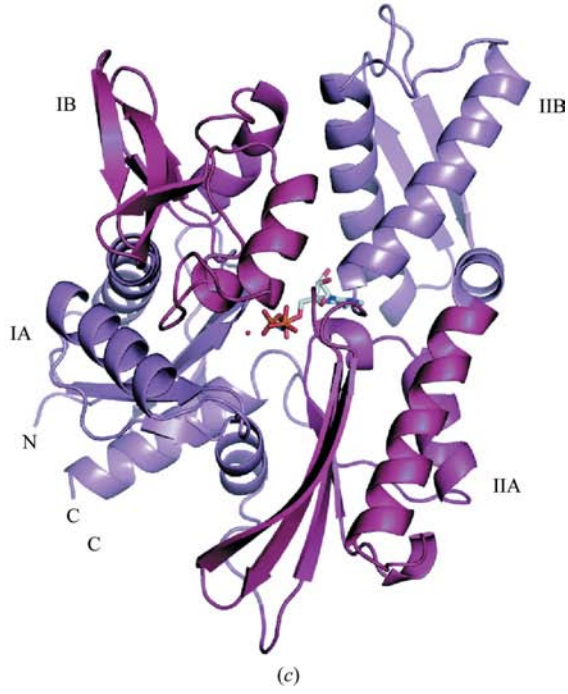

Figure 1
Structures of nucleotide-free NBD and AMPPNP-bound NBD. (*a*) Neither ATP nor ADP was detected by HPLC in the present nucleotide-free sample of the NBD fragment of human Hsp70. Top plot, 20 µ*M* NBD purified with a HiTrap Blue column (blue); middle plot, 20 µ*M* NBD purified without the HiTrap Blue column (black); bottom plot, 20 µ*M* ATP (red) and 20 µ*M* ADP (black). (*b*) The crystal structure of the human Hsp70 nucleotide-free NBD. The black ball indicates the Zn^{2+} ion. (*c*) The crystal structure of the AMPPNP-bound NBD. The white-based stick model represents AMPPNP and the red ball represents the Mg^{2+} ion. The NBD is composed of four subdomains: IA (residues 3–39, 116–188 and 361–384), IB (residues 40–115), IIA (residues 189–228 and 307–360) and IIB (residues 229–306). All of the graphic figures in this paper were produced using the program *PyMOL* (DeLano Scientific, USA).

the AMPPNP-bound NBD, with a root-mean-square deviation (r.m.s.d.) of 0.7 Å for all protein atoms. In addition, both the nucleotide-free and AMPPNP-bound NBD structures are similarly superimposable on the previously reported ADP-bound NBD structure in the closed form, with r.m.s.d.s of 1.0 and 0.7 Å, respectively. Furthermore, we noticed that a nucleotide-free NBD structure of bovine Hsc70 (PDB code 2qw9, chain *A*; Jiang *et al.*, 2007) exhibited a similarly small r.m.s.d. (1.1 Å) from the present nucleotide-free NBD structure.

As for the nucleotide-free state, open-form structures have also been reported for the Hsc70 NBD fragment complexed with the BAG domain (PDB code 1hx1; NBD–BAG; Sondermann *et al.*, 2001), the Hsc70 fragment containing both the NBD and SBD (PDB code 1yuw; nucleotide-free NBD-SBD; Jiang *et al.*, 2005) and the Hsp70 NBD fragment complexed with ATP-bound Sse1 protein (PDB code 3d2f; NBD–Sse1; Polier *et al.*, 2008). The r.m.s.d.s from the present nucleotide-free NBD structure are 1.7,

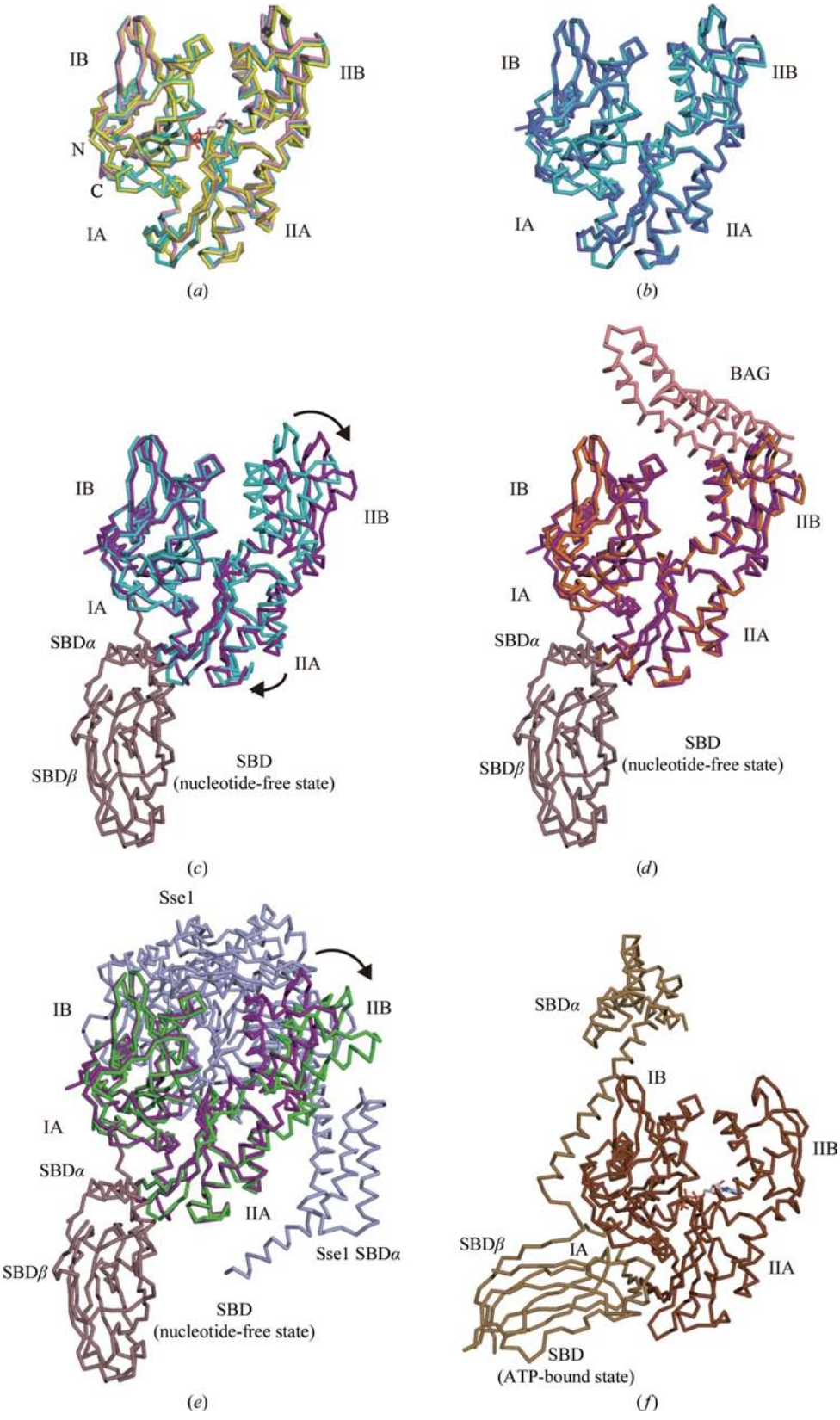

Figure 2
The closed-form NBD structures in comparison with the open/open*-form structures. We superimposed the NBDs with respect to subdomain IA. (*a*) Superimposition of the NBDs in the nucleotide-free state (cyan; nucleotide-free NBD), in complex with AMPPNP (pink; AMPPNP-bound NBD) and in complex with ADP (yellow; PDB code 1hjo; ADP-bound NBD). The white-based stick model indicates AMPPNP. (*b*) Superimposition of the nucleotide-free NBD and the previously reported NBD in the nucleotide-free state (slate; PDB code 2qw9). (*c*) Superimposition of the nucleotide-free NBD and bovine Hsc70 containing both the NBD and the SBD in the nucleotide-free state (purple; PDB code 1yuw; nucleotide-free NBD-SBD). (*d*) Superimposition of the nucleotide-free NBD-SBD and the NBD in complex with the BAG domain from BAG-1 (PDB code 1hx1; NBD–BAG). For NBD–BAG, the NBD is shown in orange and the BAG domain is coloured salmon pink. (*e*) Superimposition of the nucleotide-free NBD-SBD and NBD in complex with Sse1 (PDB code 3d2f; NBD–Sse1). For NBD–Sse1, the NBD is shown in green and Sse1 is shown in light blue. (*f*) The crystal structure of Sse1 in the ATP-bound state (brown; PDB code 2qxl; ATP-bound NBD-SBD). The stick model represents ATP.

2.1 and 3.2 Å for the nucleotide-free NBD-SBD, NBD–BAG and NBD–Sse1 structures, respectively, which are much larger than those for the nucleotide-bound NBD structures.

These structural differences primarily arise from variations in the relative arrangement of the four subdomains, which may be compared by superposition of subdomain IA (Fig. 2) using the program *LSQKAB* (Kabsch, 1976; Collaborative Computational Project, Number 4, 1994). Thus, the r.m.s.d.s from the present nucleotide-free NBD structure amount to 0.8, 1.4 and 1.2 Å for the AMPPNP-bound NBD, ADP-bound NBD and previous nucleotide-free NBD structures (Figs. 2*a* and 2*b*), respectively, while they amount to 2.4, 2.8 and 5.4 Å for the nucleotide-free NBD-SBD, NBD–BAG and NBD–Sse1 structures (Figs. 2*c*, 2*d* and 2*e*), respectively.

3.4. Nucleotide-binding pocket structures

Most of the nucleotide-binding residues in the nucleotide-free NBD are in positions quite similar to those in the AMPPNP-bound NBD (Fig. 3*a*). For the previously reported structure of the nucleotide-free NBD (PDB code 2qw9, chain *A*; Jiang *et al.*, 2007) most of the nucleotide-binding residues superimposed well (Fig. 3*b*). On the other hand, the nucleotide-binding residues in the nucleotide-free NBD-SBD structure are in different positions to those in the nucleotide-free NBD structure; the nucleotide-binding pocket of the nucleotide-free NBD-SBD is much wider than that of the nucleotide-free NBD (Fig. 3*c*). In contrast, when NBD–BAG and the nucleotide-free NBD-SBD were compared the nucleotide-binding pockets superimposed well (Fig. 3*d*). Thus, the overall structure of the nucleotide-free NBD, including the nucleotide-binding residues, is different from those of the nucleotide-free NBD-SBD and NBD–BAG. Therefore, like the AMPPNP-bound NBD structure, the present nucleotide-free NBD structure is designated as the closed form, whereas the nucleotide-free NBD-SBD and NBD–BAG structures are in the open form. Furthermore, the nucleotide-binding pocket of NBD–Sse1 is wider than that of the nucleotide-free NBD-SBD (the 'open* form'; Fig. 3*e*).

On the other hand, the NBD and SBD structures of the ATP-bound Sse1 with and without Hsp70/Hsc70 NBD (Liu & Hendrickson, 2007; Polier *et al.*, 2008; Schuermann *et al.*, 2008) may be compared with those of Hsp70. The conformation of the NBD portion in the ATP-bound Sse1 is the closed form, which does not significantly differ from the AMPPNP-bound structure of the Hsp70 NBD in the closed form (Fig. 3*f*). In the ATP-bound Sse1 structure the locations of the SBDα and

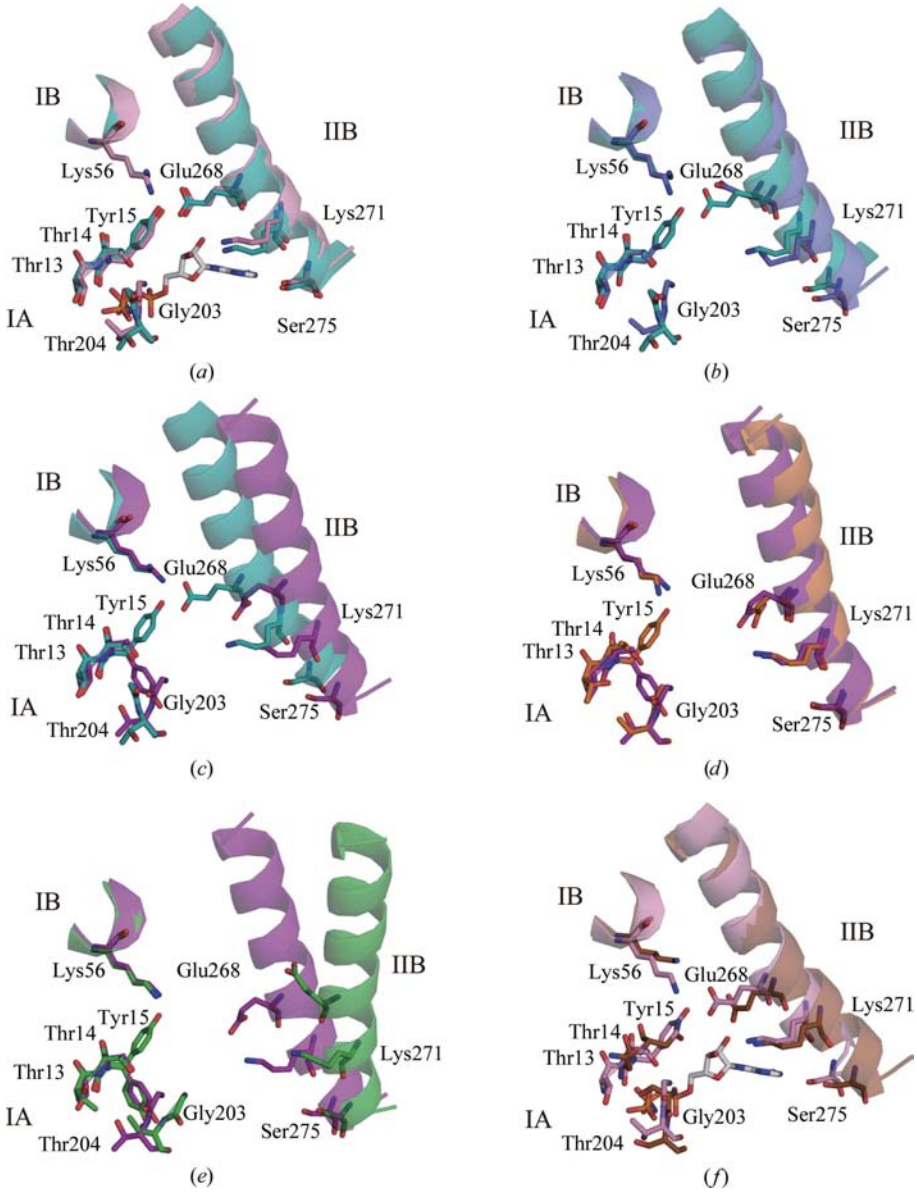

Figure 3
The central part of the NBD. Thr13, Thr14, Tyr15, Gly203, Thr204, Lys271 and Ser275 interact with AMPPNP. Lys56 belongs to subdomain IB and Glu268 belongs to subdomain IIB. (*a*) Superimposition of the nucleotide-free NBD (cyan) and the AMPPNP-bound NBD (pink). The white-based stick model represents AMPPNP. (*b*) Superimposition of the nucleotide-free NBD and the previously reported nucleotide-free NBD (slate). (*c*) Superimposition of the nucleotide-free NBD and the nucleotide-free NBD-SBD (purple). (*d*) Superimposition of the nucleotide-free NBD-SBD and NBD–BAG (orange). (*e*) Superimposition of the nucleotide-free NBD-SBD and NBD–Sse1 (green). (*f*) Superimposition of the AMPPNP-bound NBD and the ATP-bound NBD-SBD (brown). The white-based stick model shows AMPPNP.

SBDβ portions relative to each other and to the NBD portion (Fig. 2*f*) differ dramatically from those in the nucleotide-free NBD-SBD of Hsp70 (Fig. 2*c*).

3.5. Inter-subdomain interactions that characterize the closed form

Next, we examined why the NBD fragment is able to assume the closed form in the absence of ATP or ADP. The present and previous nucleotide-free NBD structures in the closed form exhibit different modes of crystal packing, indicating that the closed form of the nucleotide-free NBD is not a consequence of crystal packing. In the case of *E. coli* DnaK, electrostatic interactions or salt bridges between Lys55 and Glu267 and between Arg56 and Glu264 prevent release of the adenine nucleotide (Brehmer *et al.*, 2001). The Lys55 and Glu267 residues are conserved in eukaryotic Hsp70 and correspond to Lys56 and Glu268, respectively, in human Hsp70. In our nucleotide-free NBD structure Glu268 from subdomain IIB forms a hydrogen bond to Tyr15 from subdomain IA and an electrostatic interaction with Lys56 from subdomain IB (Fig. 4*a*). In the AMPPNP-bound NBD structure Glu268 interacts similarly with Tyr15 and Lys56. In addition, a hydrogen bond is formed between Tyr15 and Lys56 (Fig. 4*b*). In the previous nucleotide-free NBD structure Glu268 does not directly contact either Tyr15 or Lys56, but interacts indirectly with them through two water molecules (Fig. 4*c*). In spite of the differences in the details, all three closed forms are characterized by the direct or water-mediated interaction of Glu268 from subdomain IIB with Tyr15 and Lys56 from subdomains IA and IB, respectively. Consequently, we concluded that these inter-subdomain interactions keep the three subdomains in the geometry defining the closed form.

In contrast, in the structure of the open-form nucleotide-free NBD-SBD Glu268 interacts with neither Tyr15 nor Lys56 (Fig. 4*d*). In the structures of other open-form NBDs, such as NBD–BAG and NBD–Sse1, Glu268 is too far away to interact with either Tyr15 or Lys56, while Tyr15 and Lys56 interact with each other (Figs. 4*e* and 4*f*). Therefore, the lack of subdomain interactions involving Glu268 is characteristic of open-form NBD structures. The direct inter-subdomain interactions occur next to the nucleotide-binding site (Fig. 3*a*) and at the centre of the NBD (Fig. 2*a*). Tyr15, Lys56 and Glu268 play a key role in controlling the position of subdomain IIB relative to subdomains IA and IB and in stabilizing the closed form, even in the absence of the nucleotide. It should be emphasized again that the closed form of the NBD is characterized not by indirect interactions mediated by the nucleotide but by direct subdomain interactions.

The nucleotide-free NBD structure determined in the present study is in the closed form and thus differs from the open-form structures of the nucleotide-free NBD-SBD and NBD–BAG and the open*-form structure of NBD–Sse1. A comparison of these structures indicated that the closed form is stabilized by the central interactions between Tyr15, Lys56 and Glu268 in either the presence or absence of ATP/AMPPNP. In the closed-form NBD the central

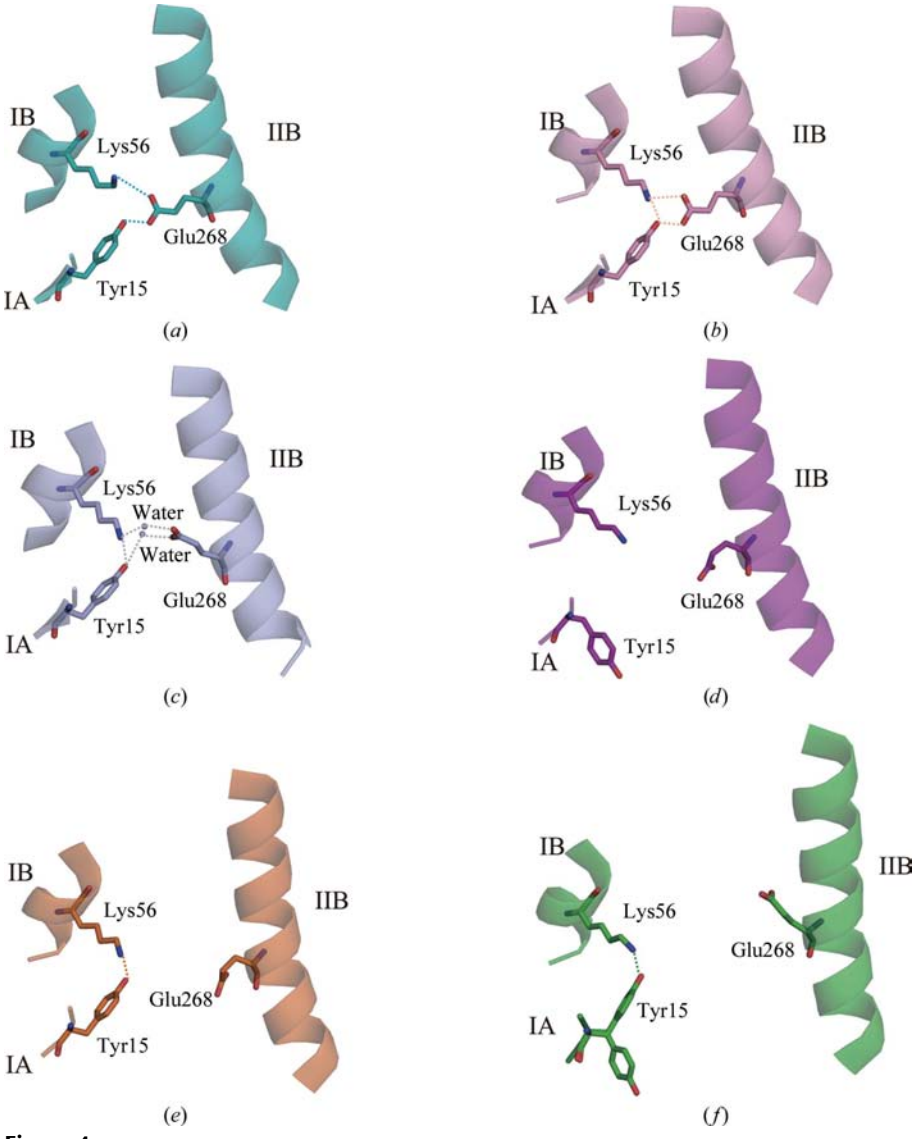

Figure 4
Glu268 interacts with Tyr15 and Lys56 in the closed-form NBD. These residues are represented as stick models. The three residues are shown in (*a*) the nucleotide-free NBD (cyan), (*b*) the AMPPNP-bound NBD (pink), (*c*) the previously reported nucleotide-free NBD (slate; the balls represent water molecules), (*d*) the nucleotide-free NBD-SBD (purple), (*e*) NBD–BAG (orange) and (*f*) NBD–Sse1 (green).

Tyr15, Lys56 and Glu268 residues fix the nucleotide-binding pocket in a form suitable for ATP binding. When ATP/AMPPNP binds to the NBD, the γ-phosphate group strongly interacts with Thr13, Thr14, Gly203 and Thr204 (Fig. 3*a*) and the closed-form NBD becomes stable. Therefore, the conformational transition towards the open form is unlikely in the ATP/AMPPNP-bound NBD. In this context, an NMR analysis has revealed that the subdomain–subdomain orientation in the NBD of *Thermus thermophilus* DnaK is more stabilized in the AMPPNP-bound form than in the ADP-bound form (Bhattacharya *et al.*, 2009).

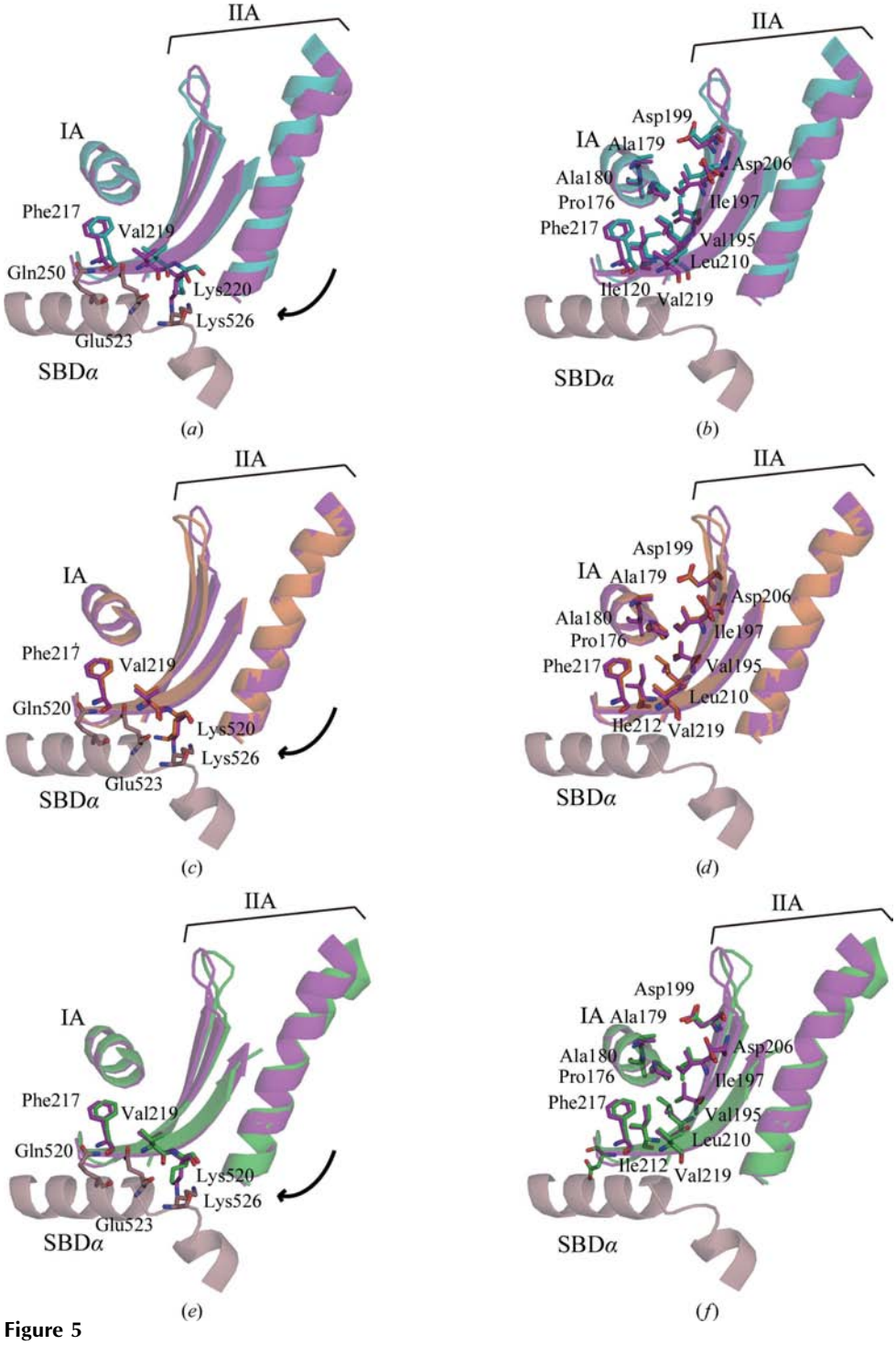

Figure 5
Subdomain IIA shifts towards the SBD in the open-form NBD. (*a*, *b*) Superimposition of the nucleotide-free NBD (cyan) and the nucleotide-free NBD-SBD (purple). (*c*, *d*) Superimposition of the nucleotide-free NBD-SBD and NBD–BAG (orange). (*e*, *f*) Superimposition of the nucleotide-free NBD-SBD and NBD–Sse1 (green). (*a*), (*c*) and (*e*) highlight the interface between subdomain IIA and the SBD, with the interacting residues shown as stick models, while (*b*), (*d*) and (*f*) highlight the interface between subdomains IA and IIA.

3.6. Inter-subdomain interactions characteristic of the open-form NBD

Next, we examined how the NBDs interacting with the SBD and the BAG domain assume the well defined open form. In the nucleotide-free NBD-SBD structure SBDα interacts with subdomains IA and IIA. Compared with the closed form, subdomain IIA is shifted by about 1 Å towards SBDα, so that a line of residues on the β-strand at the edge of subdomain IIA are just within suitable distances to hydrogen bond to the residues lined up on an α-helical segment of SBDα (Fig. 5*a*). The interaction with SBDα causes the β-sheet of subdomain IIA to rotate clockwise around an α-helix from subdomain IA (Fig. 5*b*). The surfaces of both the subdomain IIA β-sheet and the subdomain IA α-helix contain many hydrophobic amino-acid residues, allowing the smooth rotation. Rotation of subdomain IIA is also observed in the NBD–BAG structure (Fig. 5*d*). The structures of the SBDα-interacting residues and those around the interface between subdomains IA and IIA are perfectly superimposable in the nucleotide-free NBD-SBD and the NBD–BAG structures (Fig. 5*c*). Therefore, even when the BAG domain binds to a distant part of the NBD, the arrangement of subdomains IA and IIA becomes exactly suitable for binding to SBDα. In turn, when the SBDα interacts with subdomains IA and IIA the other end of the NBD becomes 'open' and appropriate for interaction with the BAG domain. Furthermore, the arrangement of sub-

domains IA and IIA in the NBD–Sse1 structure also corresponds to that in the nucleotide-free NBD-SBD structure, although the NBD–Sse1 structure is the open* form (Figs. 5*e* and 5*f*). Therefore, the open and open* forms exhibit a different arrangement of subdomains IIA and IIB but almost the same arrangement of subdomains IA and IIA. Taken together, these structural features indicate that the rotation of subdomain IIA around the subdomain IA α-helix is strictly regulated to the same extent.

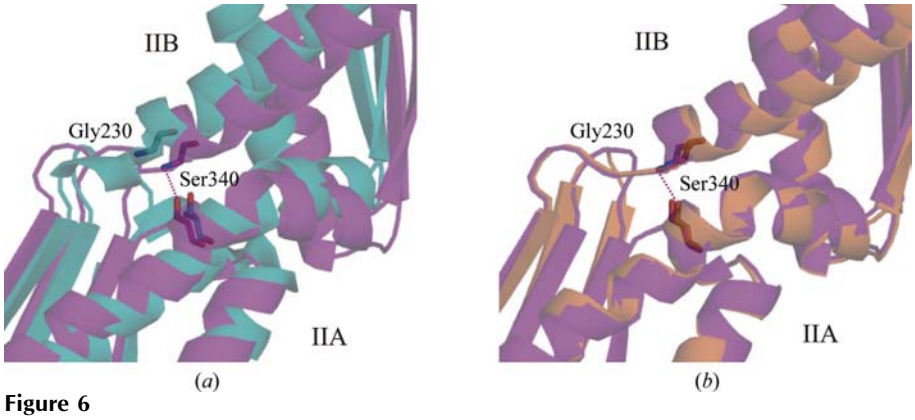

Figure 6
The interaction between Gly230 and Ser340 fixes subdomain IIB on subdomain IIA and stabilizes the open-form NBD. (*a*) Superimposition of the nucleotide-free NBD and the nucleotide-free NBD-SBD, focusing on the region between subdomains IIA and IIB. (*b*) Superimposition of the nucleotide-free NBD-SBD and NBD–BAG.

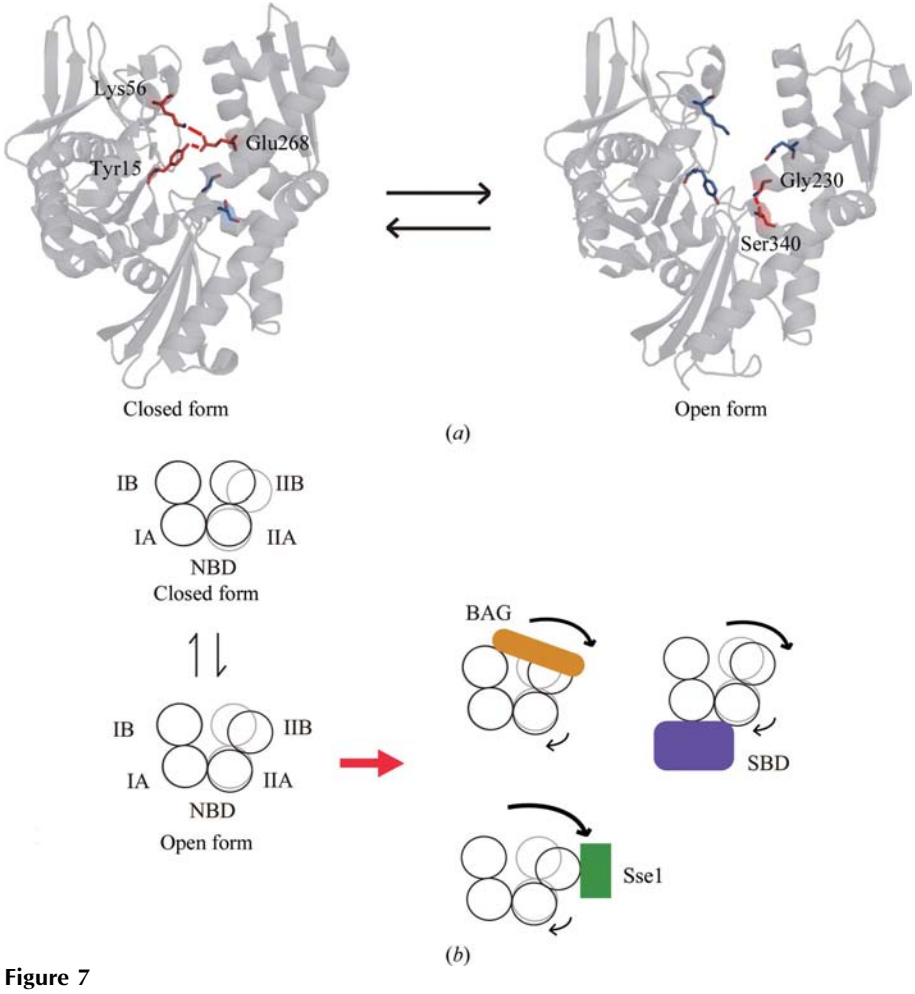

Figure 7
The NBD is in equilibrium between the closed and open forms. (*a*) The intersubdomain interaction between Tyr15, Lys56 and Glu268 characterizes the closed form, whereas that between Gly230 and Ser340 characterizes the open form. The red-based stick models show interacting residues and the blue-based stick models represent non-interacting residues. (*b*) The SBD, the BAG domain and Sse1 keep the NBD in the open form.

Therefore, we looked for the putative 'limiter' for the rotation and found Asp199 and Asp206 next to the hydrophobic surface of the β-sheet. If the rotation goes too far then these charged residues would be able to interact with the hydrophobic surface of the subdomain IA α-helix. Therefore, we propose here that the pair of Asp residues serves to limit the rotation to precisely construct the open form suitable for the SBDα interaction.

In the open-form NBD structure the rotation of subdomain IIA separates subdomain IIB from subdomains IA and IB and Glu268 is thus unable to interact with Tyr15 and Lys56, respectively. On the other hand, in the structures of the nucleotide-free NBD-SBD and NBD–BAG the main-chain NH group of Gly230 from subdomain IIB newly interacts with the side-chain hydroxyl group of Ser340 from subdomain IIA. This interaction fastens subdomain IIB on subdomain IIA and stabilizes the open form of the NBD (Figs. 6*a* and 6*b*). On the other hand, this interaction is not observed in the present nucleotide-free NBD structure in the closed form because subdomain IIB interacts with subdomains IA and IB and Gly230 is about 5.9 Å farther from Ser340 (Fig. 6*a*). Consequently, the interaction between subdomains IIA and IIB is also important for maintenance of the defined open form of the NBD.

4. Conclusion

The nucleotide-free NBD exists in an equilibrium between the closed form, which is characterized by the interactions between Tyr15, Lys56 and Glu268, and the open form, which is associated with the interaction between Gly230 and Ser340 (Fig. 7*a*). In the closed form the central Tyr15, Lys56 and Glu268 residues fix the arrangement of the subdomains and therefore the

nucleotide-binding pocket is suitable for ATP binding. The equilibrium between the open and closed forms is likely to be shifted towards the open form upon interaction with the SBD, the BAG domain or Sse1 (Fig. 7*b*). In the NBD in the open/open* form, Asp199 and Asp206 limit the rotation to keep the subdomains in the appropriate positions. Furthermore, Gly230 and Ser340 interact between subdomains IIA and IIB to perfectly fix their relative positions in the open-form NBD, *i.e.* the nucleotide-free NBD-SBD and NBD–BAG.

We thank Dr T. Terada, Dr T. Kaminishi, Mr M. Kawazoe, Mr A. Tuerxun and Mr R. Akasaka for helpful advice. We are grateful to Ms A. Ishii and Ms T. Nakayama for clerical assistance. We also thank the administrators at SPring-8 BL26B2 for data collection. This work was supported by the RIKEN Structural Genomics/Proteomics Initiative (RSGI), the National Project on Protein Structural and Functional Analysis, Ministry of Education, Culture, Sports, Science and Technology of Japan.

References

Bertelsen, E. B., Chang, L., Gestwicki, J. E. & Zuiderweg, E. R. (2009). *Proc. Natl Acad. Sci. USA*, **106**, 8471–8476.
Bhattacharya, A., Kurochkin, A. V., Yip, G. N., Zhang, Y., Bertelsen, E. B. & Zuiderweg, E. R. (2009). *J. Mol. Biol.* **388**, 475–490.
Brehmer, D., Rüdiger, S., Gässler, C. S., Klostermeier, D., Packschies, L., Reinstein, J., Mayer, M. P. & Bukau, B. (2001). *Nature Struct. Biol.* **8**, 427–432.
Brünger, A. T., Adams, P. D., Clore, G. M., DeLano, W. L., Gros, P., Grosse-Kunstleve, R. W., Jiang, J.-S., Kuszewski, J., Nilges, M., Pannu, N. S., Read, R. J., Rice, L. M., Simonson, T. & Warren, G. L. (1998). *Acta Cryst.* D**54**, 905–921.
Chang, Y.-W., Sun, Y.-J, Wang, C. & Hsiao, C.-D. (2008). *J. Biol. Chem.* **283**, 15502–15511.
Chou, C.-C., Forouhar, F., Yeh, Y.-H., Shr, H.-L., Wang, C. & Hsiao, C.-D. (2003). *J. Biol. Chem.* **278**, 30311–30316.
Collaborative Computational Project, Number 4 (1994). *Acta Cryst.* D**50**, 760–763.
Cupp-Vickery, J. R., Peterson, J. C., Ta, D. T. & Vickery, L. E. (2004). *J. Mol. Biol.* **342**, 1265–1278.
DiDomenico, B. J., Bugaisky, G. E. & Lindquist, S. (1982). *Proc. Natl Acad. Sci. USA*, **79**, 6181–6185.
Easton, D. P., Kaneko, Y. & Subjeck, J. R. (2000). *Cell Stress Chaperones*, **5**, 276–290.
Emsley, P. & Cowtan, K. (2004). *Acta Cryst.* D**60**, 2126–2132.
Flaherty, K. M., DeLuca-Flaherty, C. & McKay, D. B. (1990). *Nature (London)*, **346**, 623–628.
Flaherty, K. M., Wilbanks, S. M., DeLuca-Flaherty, C. & McKay, D. B. (1994). *J. Biol. Chem.* **269**, 12899–12907.
Goldfarb, S. B., Kashlan, O. B., Watkins, J. N., Suaud, L., Yan, W., Kleyman, T. R. & Rubenstein, R. C. (2006). *Proc. Natl Acad. Sci. USA*, **103**, 5817–5822.
Ha, J. H. & McKay, D. B. (1994). *Biochemistry*, **33**, 14625–14635.
Hantschel, M., Pfister, K., Jordan, A., Scholz, R., Andreesen, R., Schmitz, G., Schmetzer, H., Hiddemann, W. & Multhoff, G. (2000). *Cell Stress Chaperones*, **5**, 438–442.
Harrison, C. J., Hayer-Hartl, M., Di Liberto, M., Hartl, F. & Kuriyan, J. (1997). *Science*, **276**, 431–435.
Hunt, C. & Morimoto, R. I. (1985). *Proc. Natl Acad. Sci. USA*, **82**, 6455–6459.
Imai, Y., Soda, M., Hatakeyama, S., Akagi, T., Hashikawa, T., Nakayama, K. I. & Takahashi, R. (2002). *Mol. Cell*, **10**, 55–67.
Jaattela, M. (1993). *J. Immunol.* **151**, 4286–4294.
Jiang, J., Maes, E. G., Taylor, A. B., Wang, L., Hinck, A. P., Lafer, E. M. & Sousa, R. (2007). *Mol. Cell*, **28**, 422–433.
Jiang, J., Prasad, K., Lafer, E. M. & Sousa, R. (2005). *Mol. Cell*, **20**, 513–524.
Kabsch, W. (1976). *Acta Cryst.* A**32**, 922–923.
Kalia, S. K., Lee, S., Smith, P. D., Liu, L., Crocker, S. J., Thorarinsdottir, T. E., Glover, J. R., Fon, E. A., Park, D. S. & Lozano, A. M. (2004). *Neuron*, **44**, 931–945.
Kao, H. T., Capasso, O., Heintz, N. & Nevins, J. R. (1985). *Mol. Cell. Biol.* **5**, 628–633.
Laskowski, R. A., MacArthur, M. W., Moss, D. S. & Thornton, J. M. (1993). *J. Appl. Cryst.* **26**, 283–291.
Lindquist, S. & Craig, E. A. (1988). *Annu. Rev. Genet.* **22**, 631–677.
Liu, Q. & Hendrickson, W. A. (2007). *Cell*, **131**, 106–120.
Mayer, M. P., Schröder, H., Rüdiger, S., Paal, K., Laufen, T. & Bukau, B. (2000). *Nature Struct. Biol.* **7**, 586–593.
Millar, D. G., Garza, K. M., Odermatt, B., Elford, A. R., Ono, N., Li, Z. & Ohashi, P. S. (2003). *Nature Med.* **9**, 1469–1476.
Morshauser, R. C., Hu, W., Wang, H., Pang, Y., Flynn, G. C. & Zuiderweg, E. R. (1999). *J. Mol. Biol.* **289**, 1387–1403.
Multhoff, G., Mizzen, L., Winchester, C. C., Milner, C. M., Wenk, S., Eissner, G., Kampinga, H. H., Laumbacher, B. & Johnson, J. (1999). *Exp. Hematol.* **27**, 1627–1636.
Niedzwiecki, A., Kongpachith, A. M. & Fleming, J. E. (1991). *J. Biol. Chem.* **266**, 9332–9338.
Nylandsted, J., Rohde, M., Brand, K., Bastholm, L., Elling, F. & Jaattela, M. (2000). *Proc. Natl Acad. Sci. USA*, **97**, 7871–7876.
O'Brien, M. C., Flaherty, K. M. & McKay, D. B. (1996). *J. Biol. Chem.* **271**, 15874–15878.
Osipiuk, J., Walsh, M. A., Freeman, B. C., Morimoto, R. I. & Joachimiak, A. (1999). *Acta Cryst.* D**55**, 1105–1107.
Otwinowski, Z. & Minor, W. (1997). *Methods Enzymol.* **276**, 307–326.
Pellecchia, M., Montgomery, D. L., Stevens, S. Y., Vander Kooi, C. W., Feng, H. P., Gierasch, L. M. & Zuiderweg, E. R. (2000). *Nature Struct. Biol.* **7**, 298–303.
Polier, S., Dragovic, Z., Hartl, F. U. & Bracher, A. (2008). *Cell*, **133**, 1068–1079.
Raviol, H., Sadlish, H., Rodriguez, F., Mayer, M. P. & Bukau, B. (2006). *EMBO J.* **25**, 2510–2518.
Schuermann, J. P., Jiang, J., Cuellar, J., Llorca, O., Wang, L., Gimenez, L. E., Jin, S., Taylor, A. B., Demeler, B., Morano, K. A., Hart, P. J., Valpuesta, J. M., Lafer, E. M. & Sousa, R. (2008). *Mol. Cell*, **31**, 232–243.
Sondermann, H., Scheufler, C., Schneider, C., Hohfeld, J., Hartl, F. U. & Moarefi, I. (2001). *Science*, **291**, 1553–1557.
Sriram, M., Osipiuk, J., Freeman, B., Morimoto, R. & Joachimiak, A. (1997). *Structure*, **5**, 403–414.
Swain, J. F., Dinler, G., Sivendran, R., Montgomery, D. L., Stotz, M. & Gierasch, L. M. (2007). *Mol. Cell*, **26**, 27–39.
Ungewickell, E., Ungewickell, H. & Holstein, S. E. (1997). *J. Biol. Chem.* **272**, 19594–19600.
Vagin, A. & Teplyakov, A. (1997). *J. Appl. Cryst.* **30**, 1022–1025.
Wang, H., Kurochkin, A. V., Pang, Y., Hu, W., Flynn, G. C. & Zuiderweg, E. R. (1998). *Biochemistry*, **37**, 7929–7940.
Wilbanks, S. M., Chen, L., Tsuruta, H., Hodgson, K. O. & McKay, D. B. (1995). *Biochemistry*, **34**, 12095–12106.
Xu, Z., Page, R. C., Gomes, M. M., Kohli, E., Nix, J. C., Herr, A. B., Patterson, C. & Misra, S. (2008). *Nature Struct. Mol. Biol.* **15**, 1309–1317.
Zakeri, Z. F. & Wolgemuth, D. J. (1987). *Mol. Cell. Biol.* **7**, 1791–1796.
Zhu, X., Zhao, X., Burkholder, W. F., Gragerov, A., Ogata, C. M., Gottesman, M. E. & Hendrickson, W. A. (1996). *Science*, **272**, 1606–1614.